International Journal of Modern Physics E
Vol. 26, Nos. 1 & 2 (2017) 1740003 (12 pages)

DOI: 10.1142/S0218301317400031

World Scientific
www.worldscientific.com

The oxygen isotopes

B. Alex Brown

Department of Physics and Astronomy
and National Superconducting Cyclotron Laboratory
Michigan State University, East Lansing,
Michigan 48824-1321, USA

Published 26 January 2017

The properties of the oxygen isotopes provide diverse examples of progress made in experiments and theory. This chain of isotopes has been studied from beyond the proton drip line in ^{12}O to beyond the neutron drip line in ^{25,26}O. This short survey starts with the microscopic G matrix approach for ^{18}O of Kuo and Brown in the 1960's and shows how theory has evolved. The nuclear structure around the doubly-magic nucleus ^{24}O is particularly simple in terms of the nuclear shell model. The nuclear structure around the doubly-magic nucleus ^{16}O exhibits the coexistence of single-particle and collective structure.

Keywords: Shell model; oxygen isotopes.

PACS Number(s): 21.10.−k, 21.60.Cs, 27.10.+n, 27.30.+t, 29.30.Hs

1. Introduction

The properties of the oxygen isotopes provide diverse examples of progress made in experiment and theory. The known isotopes are shown in Fig. 1. There are three stable isotopes ^{16,17,18}O. Due to the temperature-dependent effect of the mass difference on evaporation and condensation, measurement of the changes in the isotopic ratio ^{18}O/^{16}O in ice cores provides information on historic climate changes.[1] With the advent of radioactive beams, there is now a nearly complete set of data known for all of the oxygen isotopes.[2] ^{12}O lies beyond the proton drip line and is observed to decay by emission of two protons ^{25}O lies beyond the neutron drip line and is observed to decay by the emission of one neutron. ^{26}O lies even further beyond the neutron drip line and is observed to decay by the emission of two neutrons. The root-mean-square (RMS) charge radii and charge form factors for the stable isotopes have been measured with electron scattering.[2] The RMS matter radii for ground states out to ^{24}O have been measured from interaction cross-sections[3,4] and elastic proton scattering.[5–7]

The properties of ^{16,17,18}O provided the first ingredients for the formulation of nuclear theory in terms of configuration–interaction (CI) models. $Z = 8$ is a magic

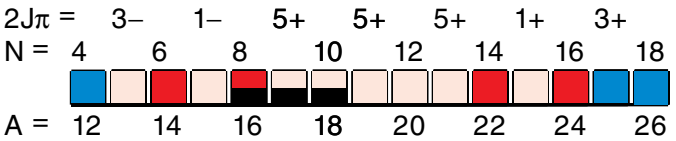

Fig. 1. (Color online) The oxygen isotopes. A is the mass number and N is the neutron number. $2J\pi$ is the ground state spin-parity for the ground states of the odd-neutron nuclei. The black rectangles show the three stable isotopes. The blue squares are those nuclei that are observed to be beyond the proton (left) and neutron (right) drip lines. The red squares are the doubly-magic even–even nuclei.

number for all of the oxygen isotopes except ^{12}O. There are three strongly doubly-magic nuclei ^{14,16,24}O ($N = 6, 8, 16$) shown in dark red in Fig. 1, all with first excited states above 4 MeV, and a weaker doubly-magic nucleus, ^{22}O ($N = 14$), with a first excited state at 3.2 MeV shown in dark red. In the shell model, the magic number arises when the neutron shell gaps at these neutron numbers are larger than two times the pairing gap.[8] This is the start of a rich doubly-magic number sequence observed up to ^{54}Ca.[9,10] The ground state spin of the odd–even nuclei shown in Fig. 1 are all explained by the sequential filling of the shell-model orbitals $0p_{3/2}(3/2^-)$, $0p_{1/2}(1/2^-)$, $0d_{5/2}(5/2^+)$, $1s_{1/2}(1/2^+)$ and $0d_{3/2}(3/2^+)$.

2. Structure for the *sd* Model Space Based on the Free Nucleon–Nucleon Interaction

I was a graduate student at Stony Brook from 1970–1973 working on experiments with my adviser Dave Fossen. During that time, I took several courses in nuclear theory, and had many interactions with Brown's nuclear theory group and their visitors. I will start the theory part of this review with the work of Kuo and Brown in the late 1960's.[11–15] Kuo and Brown planted many trees which have matured and left their seeds for the growth of nuclear theory. Their goal was to investigate the applicability of the free nucleon–nucleon potential determined by the scattering data for the shell-model description of finite nuclei. The first example they gave was for ^{18}O, where they started with a doubly closed-shell configuration for ^{16}O and calculated the spectrum of ^{18}O in the $(1s_{1/2}, 0d_{5/2}, 0d_{3/2})$ *sd* model space. The Brueckner reaction matrix G for the scattering of two nucleons evaluated with various methods was used to take into account the repulsive short-ranged part of the potential. The method of second-order core-polarization was used to renormalize the G-matrix elements into the *sd* model space. The end result was a set of two-body matrix elements (TBME) (63 of them) for the *sd* model space[15] that could be diagonalized to obtain the energies of ^{18}O relative to that of ^{16}O. The resulting energy spectrum is shown in Fig. 2 and compared to experiment. The agreement was excellent for some levels, but there are more levels observed in experiment compared to those calculated. These extra levels come from the excitation of protons from the p shell to the *sd* shell. There is mixing between these two sets,[16] but not enough

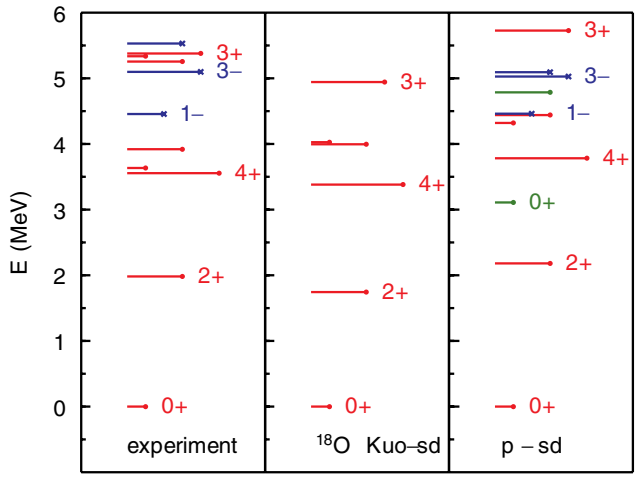

Fig. 2. (Color online) Energy levels for ^{18}O. Experiment is shown in the left-hand side with red lines for positive parity states and blue lines for negative parity states. The length of the line is proportional to the J value with a few lines labeled for reference. The middle panel shows the spectrum for positive parity states obtained with the Kuo–Brown Hamiltonian. The right-hand side shows the spectrum based on the WBP Hamiltonian from Ref. 17 that shows the *sd*-shell positive parity states (red), the $3p$-$1h$ negative parity states (blue) and the $4p$-$2h$ positive parity states (green).

to destroy the agreement for those dominated by *sd*. As one adds neutrons, these core-excited states move to higher energy. The Kuo–Brown TBME gave a starting point for the *sd* shell-model calculations beyond ^{18}O.

When the Kuo–Brown TBME are used for more neutron-rich oxygen isotopes, the agreement of the calculated spectra with experiment deteriorates. The reason for this can be understood from a plot of the of effective-single particle energies (ESPE) calculated relative to the closed-shell configurations $(0d_{5/2})^6$ for ^{22}O ($N = 14$), $(0d_{5/2})^6(1s_{1/2})^2$ for ^{24}O ($N = 16$) and $(0d_{5/2})^6(1s_{1/2})^2(0d_{3/2})^4$ for ^{28}O ($N = 28$). These are shown on the left-hand side of Fig. 3. The red dots indicate the position of the Fermi surface. The small gap at $N = 14$ means that the spectrum of the $(sd)^6$ calculation for ^{22}O does not have a closed-shell behavior in contradiction to experiment. The negative energy of the red dot at $N = 20$ means that ^{28}O is bound to neutron decay in contradiction to experiment.

There have been two paths for correcting this problem. The first of these started in the 1980's by showing that one could find a universal set of TBME for the *sd*-shell Hamiltonian that unify the understanding of data related to states with an *sd* shell configuration. The second path which has started more recently involves the addition of three-body interactions together with improved techniques for renormalization. The first path has led to many similar local solutions involving the TBME such as those in the pf shell.[19] The second path should eventually lead to a universal solution for all nuclei.

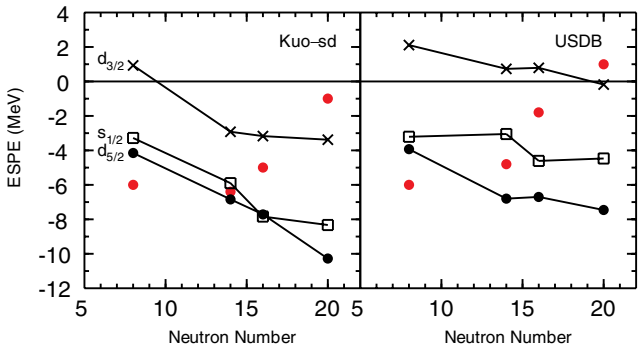

Fig. 3. (Color online) Effective single-particle energies obtained for the oxygen isotopes obtained with Kuo–Brown Hamiltonian[15] on the left and the USDB Hamiltonian[18] on the right. The orbital quantum numbers are shown on the left. The red dots indicate the position of the Fermi surface.

3. The USD Hamiltonians

In the first method, known experimental data for binding energies and excitation energies are used to obtain empirical constraints on values of the TBME. The single-valued decomposition (SVD) method is used to find $n < 63$ linear combinations of TBME that are well determined by the data. The remaining linear combinations are fixed at the values given by the Kuo–Brown Hamiltonian. This first SVD fit was carried out by Chung[20] and Wildenthal.[21] Since one set of TBME could describe the properties of all states dominated by the *sd* shell configuration in nuclei with $A = 18$ to $A = 38$ this was called the universal *sd* (USD) interaction (W in the NuShellX Hamiltonian library[22]). The USD Hamiltonian was used to calculate observables for all *sd* shell nuclei.[23]

In 2006, an updated set of experimental energy data was used to obtain two new universal interactions, USDA and USDB.[18] This used about 600 data from $A = 17$ to $A = 40$. USDA is based on 30 SDV combinations, and USDB is based on 56 SDV combinations. The ESPE shown on the right-hand side of Fig. 3 are based on USDB. Compared to Kuo–Brown, one finds a shell gap at $N = 14$ and the Fermi surface for $N = 20$ is near zero. In the following, I will compare some experimental results to those obtained with USDB. The energies of states obtained with USDA are the same as those with USDB to within about 100 keV.

The binding energy of states in $^{22-28}$O (relative to ^{16}O) obtained with USDB are shown by the horizontal lines in Fig. 4. The data known in 2006 used to constrain the USDB TBME are shown by the three blue dots. All other horizontal lines are the energies predicted for states that were not known in 2006. All of these are unbound to neutron decay as shown by the arrows. With USDB, ^{24}O lies on the neutron drip line. Since 2006 many experiments have been carried out to measure these neutron decays. The experimental centroids of these decay resonances are shown by the red dots in Fig. 4. The interpretation of these results is particularly simple due to the

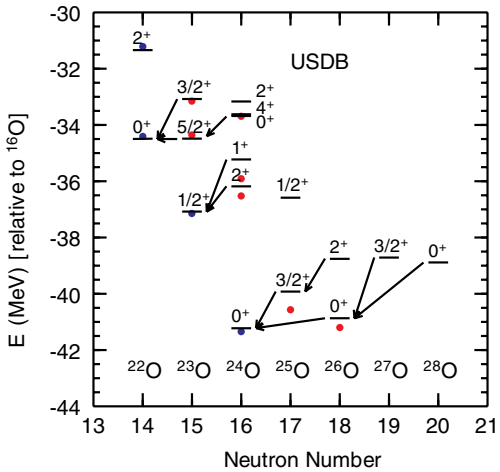

Fig. 4. (Color online) Energies of the states relative to ^{16}O as a function of mass number for the oxygen isotopes. The horizontal lines are the USDB predictions. The blue dots are experimental energies known before 2006. The arrows show the neutron decays discussed in the text. The red dots are the centroid energies observed for these neutron decays.

fact that the *sd* wave functions for these nuclei near the doubly-magic nucleus ^{24}O are dominated by simple configurations, as we will discuss below.

In 2007, an unbound level in ^{23}O consistent with a $3/2^+$ assignment was observed at RIKEN[24] that is in good agreement with the prediction. Also in 2007 a low energy neutron from the decay of ^{23}O was observed at the NSCL which was associated with the predicted $5/2^+$ state just above the neutron-decay threshold.[25] The dominant configuration for this state is $(0d_{5/2})^5(1s_{1/2})^2$, and the calculated spectroscopic factor of 0.059 is small because it must go through the $(0d_{5/2})^4(1s_{1/2})^2$ admixture into the dominant $(0d_{5/2})^6$ configuration for the ^{22}O ground state. From the observed neutron-decay centroid energy of 40 keV one predicts a neutron-decay width of 10 eV (much smaller than the experimental resolution).

In 2009, the decay of two excited states of ^{24}O were observed[26] at an energy consistent with the 2^+ and 1^+ states in Fig. 4. This experiment showed that the first excited state in ^{24}O was high (4.0 MeV) confirming the doubly closed-shell nature of ^{24}O. The centroid of these two states observed are several hundred keV lower than those predicted (2^+ and 1^+). The configuration of these two excited states is $(0d_{5/2})^6(1s_{1/2})(0d_{3/2})$. In 2012, these two states were studied with proton scattering in inverse kinematics,[27] and the measured β_2 value for the 2^+ state was found to be in good agreement with the USDB calculations. In addition a state near 7.3 MeV was observed to neutron decay which indicates it may have the configuration $(0d_{5/2})^6(1s_{1/2})(pf)$ and have negative parity. Further experimental support for the USDB 2^+ and 1^+ predictions was obtained in 2015.[28] In 2015, the two-neutron decay of a state at 7.65(20) MeV was observed.[29] This is probably one of the states shown in Fig. 2 near this energy that have the dominant configuration

$(0d_{5/2})^5(1s_{1/2})^2(0d_{3/2})$. From this configuration, one predicts a sequential decay through the $(0d_{5/2})^5(1s_{1/2})^2 5/2^+$ state in ^{23}O discussed above, in agreement with experiment.[29] The main configuration of the 0^+ state near 7.3 MeV (Fig. 3) is $(0d_{5/2})^6(0d_{3/2})^2$. It should be observed in a ^{22}O(t,p) experiment.

In 2008, the neutron decay of ^{25}O was observed[30] which was associated with the predicted $3/2^+$ state. The experimental centroid energy of this state of 770 keV is about 500 keV lower than predicted by USDB. The calculated spectroscopic factor $C^2S = 0.95$ results in a calculated neutron decay width of 79 keV (using the experimental decay Q value). The experimental width of 172(30) keV obtained in Ref. 30 is larger than that calculated, but a more recent experiment with higher statistics obtained is smaller of 88(6) keV,[31] in agreement with the prediction.

Predictions have been made for low-lying $3/2^-$ and $7/2^-$ states in ^{25}O coming from the pf shell orbitals.[32,33] The small gap between the $0d_{3/2}$ and the $1p_{3/2}-0f_{7/2}$ single-particle energies near ^{24}O is a consequence of the tensor interaction[34] together with a weak-binding effect that lowers the $1p_{3/2}$ single particle energy relative to that of $0f_{7/2}$.[35] The island of inversion[36] for nuclei near $N = 20$ and $Z \leq 12$ is due to this reduced energy gap. For these nuclei, the configurations of the type $(sd)^{n-2}(pf)^{m+2}$ come lower in energy than those for $(sd)^n(pf)^m$. A similar situation happens for $N = 8$ and $Z \leq 4$, where the shell gap between $0p_{1/2}$ and $1s_{1/2} - 0d_{5/2}$ is reduced leading to a configuration inversion in ^{12}Be (Ref. 37). This configuration inversion is also manifested in the properties[38–40] of the mirror nucleus ^{12}O that lies just beyond the proton drip line (see Fig. 1). At present, there is only a limit of 72 keV[39] on the two-proton decay width of ^{12}O.

The two neutron decay of ^{26}O–^{24}O has been observed.[31,41–43] In Ref. 42 a lifetime of 4.5(3.0) ps was obtained for this decay. In Ref. 31 the two neutrons were observed to be only 18(7) keV above threshold. The USDB prediction was 360 keV. The predictions obtained with many other theoretical models are shown in Ref. 44. Grigorenko has calculated the three-body decay of ^{26}O (Ref. 45). Based on his model, the lifetime for a decay energy of 18 keV should be on the order of 10^{-5}–10^{-3} ps. This three-body decay can provide unique insights into the two-neutron correlations. A better understanding of this three-body decay will be a challenge for future studies.

^{27,28}O have not been observed in radioactive beam experiments[46] indicating that they are neutron unbound, consistent with the *sd* shell calculations shown in Fig. 4 as well as with the calculations discussed below. But there are several low-lying resonances in ^{25}O (Ref. 33) that require a basis with the continuum. Since ^{26}O is unbound to two-neutron decay by only 18 keV one could speculate that there might be a four-neutron cluster bound state of ^{28}O. The tetra-neutron is unbound,[47] but the induced correlations in the nucleus could result in a state of ^{28}O with an extremely small binding that would make its production cross-section smaller than the limit observed experimentally.[46]

The overall agreement of experiment with the predictions of the USDB CI calculations for $^{23–26}$O is excellent. This success is due to the ability of all of the

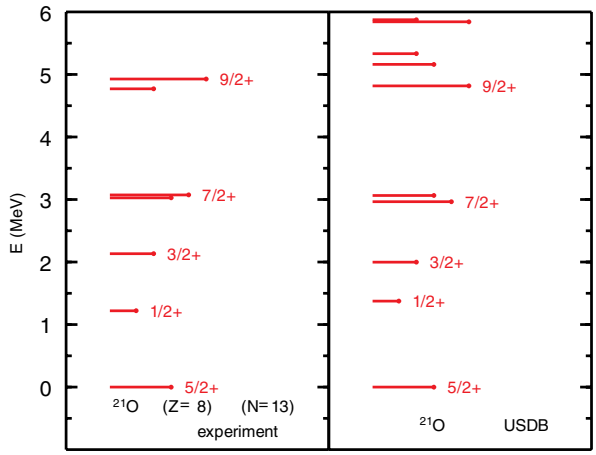

Fig. 5. Energies of the states for ^{21}O. The length of the line is proportional to the J value. The experimental results from Ref. 49 (left) are compared to the USDB predictions (right).

data related to *sd* shell configurations to be described in terms of a universal set of TBME. The TBME needed for $^{23-26}$O come from experimental energy data for $Z > 8$ as well as from excited states in $^{19-22}$O. These excited state configurations become important for the low-lying states of $^{23-26}$O. Experiments on $^{19-20}$O such as $^{18}\mathrm{O}(t,p)^{20}$ (Ref. 48), and from projectile fragmentation reactions (Ref. 49), were an important intermediate step in establishing the success of the CI calculations. The experimental results for ^{21}O obtained from Ref. 49 are compared to the USDB calculations in Fig. 5. The agreement between experiment and theory is excellent except that the $3/2^+_2$ state is about 0.5 MeV too high in theory. The $9/2^+$ state is unbound to neutron decay by 1.1 MeV. Its observation in gamma decay puts a limit of 0.029 on the spectroscopic factor for this $\ell = 4$ neutron decay (in the *sd* model space the spectroscopic factor is zero). The spectroscopic factors obtained from an $^{20}\mathrm{O}(d,p)^{21}\mathrm{O}$ experiment in inverse kinematics[50] are in good agreement with the USDB predictions.

4. The Three-Nucleon Interaction and the Development of New Theoretical Methods

In the last decade, a new class of theoretical models has been developed. Because of the relatively simple shell structure of the neutron-rich oxygen isotopes, this has been the primary testing ground for these calculations. These are similar in spirit to the original Kuo–Brown methods but expand upon them in several ways. (1) The input for the basic interaction is based upon a consistent expansion from chiral EFT in terms of two- and three-nucleon interactions.[51,52] (2) Better methods to treat short-range correlations have been developed with the $\mathrm{V}_{\mathrm{low}k}$ and free-space similarity renormalization group (SRG) approaches.[53] (3) Due to advances in the computation techniques one can include up about 15 oscillator shells in the basis.

(3) Better perturbative and non-perturbative methods have been formulated. (4) The continuum can be taken into account.[54–56] Calculations including the continuum[57] have been used to partially understand the quenching for the spectroscopic factors observed for deeply bound orbitals based upon the ratio of experimental knock-out cross-sections compared to those calculated from eikonal reaction theory with shell-model spectroscopic factors.[58]

Three-nucleon interactions are required to reproduce the magic number at ^{22}O ($N = 14$) and the position of the oxygen drip line at ^{24}O ($N = 16$).[59–62] When evaluated for an ^{16}O core, the main three-body terms are those involving the interaction of one valence neutron with two nucleons on the core, and the interaction of two valence neutrons and one nucleon in the core. This explains why effective one-plus two-body Hamiltonians of the USD type have been so successful.

Another place in the oxygen isotopes where the three-nucleon interaction is important is in the Gamow–Teller beta-decay of ^{14}O to the ground state of ^{14}N where the B(GT) is very small [B(GT) $= 3 \times 10^{-4}$].[63] The B(GT) is even smaller in the mirror transition from ^{14}C [B(GT) $= 4 \times 10^{-6}$],[63] and this results in the anomalously long half-life of 5700 years for ^{14}C that makes it so usefull for radiocarbon dating. Brown and others[64] showed that this small B(GT) can be explained by the Brown–Rho scaling model,[65,66] where the strength of the tensor interaction between nucleons is density dependent. Later it was shown that the density-dependent effects from the Brown–Rho model are similar to those from a three-nucleon force.[67] In large-basis CI calculations for ^{14}C, it was shown that the three-body interaction is important for obtaining the small B(GT) values.[68]

A commonly used input Hamiltonian due to Entem and Machleidt (EM)[51,52] is based upon an N^{3}LO two-nucleon plus a N^{2}LO three-nucleon interaction with low-energy coupling constants derived from nucleon–nucleon scattering and the properties of the $A = 3$ and $A = 4$ nuclei. The binding energies for the oxygen isotopes obtained with the EM input based on several types of non-perturbative methods[69–74] are consistent with each other and with experiment within 1–2 MeV (1% of the total binding energy). Excited states for neutron-rich nuclei from these calculations agree with each other and with experiment at the level of about 0.5 MeV. However, the intruder states in ^{18}O are not in the basis.

The RMS radii obtained with the EM interaction input is about 10% smaller than experiment for all of the oxygen isotopes.[75] This has lead to the development of a new Hamiltonian called NNLO$_{\rm sat}$ that is simpler than EM, but where the determination of the low-energy coupling constants includes data on the binding energies and charge radii of ^{14}C and ^{16,22,24,25}O as well as the charge radii of ^{14}C and ^{16}O.[76,77] The matter radii for the neutron-rich oxygen isotopes with NNLO$_{\rm sat}$ is much improved compared to experiment relative to those based on the EM input.[75] From the interaction cross-section experiments,[3,4] there is sharp increase in the matter radii between ^{22}O and ^{24}O where the $1s_{1/2}$ orbital is being filled that is only partly explained by the NNLO$_{\rm sat}$ calculations as well as by energy-density functional calculations.[78] An increase is also observed in charge radii in calcium

isotopes just after $N = 28(1p_{3/2})$,[79] the strontium isotopes just after $N = 50(1d_{5/2}$, the xenon isotopes just after $N = 82(2f_{7/2})$ and the lead isotopes just after $N = 126(2g_{9/2})$, where the given orbital is the one that starts to be filled after that magic number. All of these orbitals have an interior node whose self-consistent interactions with the core nucleons are determined by the density dependence of the equation-of-state.

Work is currently being carried out to use these non-perturbative methods to generate nucleus-dependent valence space Hamiltonians for the *sd* shell using the reference states from the targeted valence space (TVS) IM-SRG method.[80,81] It remains to be seen how or if a universal valence space Hamiltonian such as USD emerges from these calculations. Work is also started on the calculations for the nuclear moments and electromagnetic decay properties. In the CI calculations, the electric quadrupole moments and B(E2) for the oxygen isotopes depend upon the neutron effective charge which empirically is about 0.45 e.[82] [The B(E2) for ^{18}O are not well described by the *sd* shell wave functions due to the mixing with the intruder states[16,83]]. A question for the future will be to see if a universal set of low-energy coupling constants can found to reproduce experimental properties of all nuclei. If this is not the case, it may be due to real and induced four-body and higher interactions that are at present not included in the non-perturbative calculations.

5. Beyond the *sd* Shell

The methods discussed in the last section are mostly based on simple Hartree–Fock configurations for the starting point (the reference state). For example, a closed shell for ^{16}O or the $(0d_{5/2})^6$ configuration for ^{22}O. This cannot account for states whose major configuration involves core excitations. The first excited state of ^{16}O is a 0^+ state at 6.05 MeV. Its configuration is dominated by four-particles and four-holes ($4p$–$4h$) relative to the closed-shell configuration. The 0^+ state at 3.63 MeV in ^{18}O shown in Fig. 1 is dominated by a $4p$–$2h$ configuration.[16] Due to the large number or orbitals involved in these particles and holes, these intruder states are often deformed in the CI basis, and they were first discussed in terms of the Brown–Green model for coexisting spherical and deformed configurations.[84–88] Calculations have been made using the weak-coupling model where the correlations between nucleons in the same major shell are dominant and the cross-shell interaction is treated as a small perturbation.[83,89] The deformed configurations are often truncated in an SU_3 basis.[90]

Fortune used the Bansal–French–Zamick weak coupling model[91] for the $6p$–$4h$ states in ^{18}O (Ref. 92), which he suggests starts with the 0^+ state at 7.11 MeV. The success of the methods based on the spherical Hartree–Fock starting points must be that the intruder states largely decouple (coexist) with the spherical *sd* shell configurations. But this is an approximation, and ultimately one must consider both kinds of states at the same time.

Beyond the Brown–Green model, several empirical shell-model-based approaches have been made. Use of just the three orbitals $(0p_{1/2}, 0d_{5/2}, 1s_{1/2})$ closest to the Fermi surface of ^{16}O (the ZBM model space) gives a starting point and some insights.[93,94] The empirical WBP and WBT Hamiltonians[17] were developed for pure (unmixed) particle-hole configurations involving the orbitals $(0p_{3/2}, 0p_{1/2}, 0d_{5/2}, 1s_{1/2}, 0d_{3/2})$ for the mass region $A = 10$–20. The results for the $2p$, $3p$–$1h$ and $4p$–$2h$ configuration of ^{18}O are shown on the right-hand side of Fig. 2. The $2p$ (red) and $4p$–$2h$ (green) states mix,[16] leading to the experimental spectrum on the left-hand side of Fig. 2. The problem for mixing of these states due to the truncation in the np–mh sequence is discussed in Ref. 95. For the future, one might be able to use the new many-body methods to derive a Hamiltonian for the full p–sd model space as used in Ref. 96. One should also consider alpha clustering such as with the algebraic cluster model for ^{16}O which describes the strong electron scattering transitions from the ground state to the members of a $3^-, 4^+, 6^+$ (A_1) band.[97]

In summary, I have shown that the observed properties of the oxygen isotopes have provided a rich, and in some cases simple, set of observables which have been used over the past 50 years to develop and test the theories for nuclear structure. There are still problems to solve.

Acknowledgments

I acknowledge useful discussions with Heiko Hergert and support from NSF grant PHY-1404442.

References

1. K. K. Andersen *et al.*, *Nature* **431** (2004) 147.
2. http://www.nndc.bnl.gov/ensdf/.
3. A. Ozawa, T. Susuki and I. Tanihata, *Nucl. Phys. A* **693** (2001) 32.
4. R. Kanungo *et al.*, *Phys. Rev. C* **84** (2011) 061304(R).
5. E. Fabrici, S. Micheletti, M. Pignanelli, F. G. Resmini, R. De Leo, G. D'Erasmo and A. Pantaleo, *Phys. Rev. C* **21** (1980) 844.
6. E. Khan *et al.*, *Phys. Lett. B* **490** (2000) 45.
7. MUST Collab. (E. Becheva *et al.*), *Phys. Rev. Lett.* **96** (2006) 012501.
8. B. A. Brown, *Phys. Rev. Lett.* **111** (2013) 162502.
9. B. A. Brown and W. A. Richter, *Phys. Rev. C* **72** (2005) 057301.
10. D. Steppenbeck *et al.*, *Nature* **502** (2013) 207.
11. T. T. S. Kuo and G. E. Brown, *Nucl. Phys.* **85** (1966) 40.
12. T. T. S. Kuo, *Nucl. Phys. A* **90** (1967) 199.
13. R. D. Lawson, M. H. Macfarlane and T. T. S. Kuo, *Phys. Lett.* **22** (1966) 168.
14. G. E. Brown and T. T. S. Kuo, *Nucl. Phys. A* **92** (1967) 481.
15. T. T. S. Kuo, *Nucl. Phys. A* **103** (1967) 71.
16. R. L. Lawson, F. J. D. Serduke and H. T. Fortune, *Phys. Rev. C* **14** (1976) 1245.
17. E. K. Warburton and B. A. Brown, *Phys. Rev. C* **46** (1992) 923.
18. B. A. Brown and W. A. Richter, *Phys. Rev. C* **74** (2006) 034315.
19. M. Honma, T. Otsuka, B. A. Brown and T. Mizusaki, *Phys. Rev. C* **69** (2004) 034335.

20. W. Chung, Empirical renormalizations of shell-model Hamiltonians and magnetic dipole moments of sd-shell nuclei, Ph.D. thesis, Mich. State University, East Lansing (1976).
21. B. H. Wildenthal, *Prog. Part. Nucl. Phys.* **11** (1984) 5.
22. B. A. Brown and W. D. M. Rae, *Nucl. Data Sheets* **120** (2014) 115.
23. B. A. Brown and B. H. Wildenthal, *Ann. Rev. Nucl. Part. Sci.* **38** (1988) 29.
24. Z. Elekes *et al.*, *Phys. Rev. Lett.* **98** (2007) 102502.
25. A. Schiller *et al.*, *Phys. Rev. Lett.* **99** (2007) 112501.
26. C. R. Hoffman *et al.*, *Phys. Lett. B* **672** (2009) 17.
27. K. Tshoo *et al.*, *Phys. Rev. Lett.* **109** (2012) 022501.
28. W. F. Rogers *et al.*, *Phys. Rev. C* **92** (2015) 034316.
29. M. D. Jones *et al.*, *Phys. Rev. C* **92** (2015) 051306(R).
30. C. R. Hoffman *et al.*, *Phys. Rev. Lett.* **100** (2008) 152502.
31. Y. Kondo *et al.*, *Phys. Rev. Lett.* **116** (2016) 102503.
32. A. Lapailleur *et al.*, *Phys. Rev. C* **92** (2015) 054309.
33. K. Hagino and H. Sagawa, *Phys. Rev. C* **93** (2016) 034330.
34. T. Otsuka, R. Fujimoto, Y. Utsuno, B. A. Brown, M. Honma and T. Mizusaki, *Phys. Rev. Lett.* **87** (2001) 082502.
35. I. Hamamoto, *Phys. Rev. C* **76** (2007) 054319.
36. E. K. Warburton, J. A. Becker and B. A. Brown, *Phys. Rev. C* **41** (1990) 1147.
37. H. Sagawa, B. A. Brown and H. Esbensen, *Phys. Lett. B* **309** (1993) 1.
38. D. Suzuki *et al.*, *Phys. Rev. C* **93** (2016) 024316.
39. M. F. Jager *et al.*, *Phys. Rev. C* **86** (2012) 011304(R).
40. H. T. Fortune and R. Sherr, *J. Phys. G* **40** (2013) 055102.
41. E. Lunderberg, *Phys. Rev. Lett.* **108** (2012) 142503.
42. Z. Kohley *et al.*, *Phys. Rev. Lett.* **110** (2013) 152501.
43. C. Caesar *et al.*, *Phys. Rev. C* **88** (2013) 034313.
44. M. Thoennessen *et al.*, *Acta Phys. Polon. B* **44** (2013) 543.
45. L. V. Grigorenko, I. G. Mukha and M. V. Zhukov, *Phys. Rev. Lett.* **111** (2013) 042501.
46. O. Tarasov *et al.*, *Phys. Lett. B* **409** (1997) 64.
47. K. Kisamori *et al.*, *Phys. Rev. Lett.* **116** (2016) 052501.
48. S. LaFrance *et al.*, *Phys. Rev. C* **20** (1979) 1673.
49. M. Stanoiu *et al.*, *Phys. Rev. C* **69** (2004) 034312.
50. B. Fernandez-Dominguez *et al.*, *Phys. Rev. C* **84** (2011) 011301(R).
51. R. Machleidt and D. R. Entem, *Phys. Rep.* **503** (2011) 1.
52. D. R. Entem and R. Machleidt, *Phys. Rev. C* **68** (2003) 041001.
53. S. K. Bogner, R. J. Furnstahl and A. Schwenk, *Prog. Part. Nucl. Phys.* **65** (2010) 94.
54. A. Volya and V. Zelevinsky, *Phys. Rev. C* **74** (2006) 064314.
55. N. Michel, W. Nazarewicz, M. Ploszajczak and T. Vertse, *J. Phys. G* **36** (2009) 013101.
56. K. Tsukiyama, M. Hjorth-Jensen and G. Hagen, *Phys. Rev. C* **80** (2009) 051301(R).
57. O. Jensen, G. Hagen, M. Hjorth-Jensen, B. A. Brown and A. Gade, *Phys. Rev. Lett.* **107** (2011) 032501.
58. A. Gade *et al.*, *Phys. Rev. C* **77** (2008) 044306.
59. T. Otsuka, T. Suzuki, J. D. Holt, A. Schwenk and Y. Akaishi, *Phys. Rev. Lett.* **105** (2010) 032501.
60. G. Hagen, M. Hjorth-Jensen, G. R. Jansen, R. Machleidt and T. Papenbrock, *Phys. Rev. Lett.* **108** (2012) 242501.
61. J. D. Holt, J. Menendez and A. Schwenk, *Phys. Rev. Lett.* **110** (2013) 022502.
62. A. Cipollone, C. Barbieri and P. Navratil, *Phys. Rev. Lett.* **111** (2013) 062501.
63. W.-T. Chou, E. K. Warburton and B. A. Brown, *Phys. Rev. C* **47** (1993) 163.

64. J. W. Holt, G. E. Brown, T. T. S. Kuo, J. D. Holt and R. Machleidt, *Phys. Rev. Lett.* **062501** (2008).
65. G. E. Brown and M. Rho, *Phys. Rev. Lett.* **66** (1991) 2720.
66. G. E. Brown and M. Rho, *Phys. Rep.* **396** (2004) 1.
67. J. W. Holt, N. Kaiser and W. Weise, *Phys. Rev. C* **79** (2009) 054331.
68. P. Maris, J. P. Vary, P. Navratil, W. E. Ormand, H. Nam and D. J. Dean, *Phys. Rev. Lett.* **106** (2011) 202502.
69. G. R. Jansen, J. Engel, G. Hagen, P. Navratil and A. Signoracci, *Phys. Rev. Lett.* **113** (2014) 142502.
70. S. Binder, J. Langhammer, A. Calci and R. Roth, *Phys. Lett. B* **736** (2014) 119.
71. A. Cipollone, C. Barbieri and P. Navratil, *Phys. Rev. C* **92** (2015) 014306.
72. H. Hergert, S. K. Bogner, S. Binder, A. Calci, J. Langhammer, R. Roth and A. Schwenk, *Phys. Rev. C* **87** (2013) 034307.
73. H. Hergert, S. Binder, A. Calci, J. Langhammer and R. Roth, *Phys. Rev. Lett.* **110** (2013) 242501.
74. S. K. Bogner, H. Hergert, J. D. Holt, A. Schwenk, S. Binder, A. Calci, J. Langhammer and R. Roth, *Phys. Rev. Lett.* **113** (2014) 142501.
75. V. Lapoux, V. Soma, C. Barbieri, H. Hergert, J. D. Holt and S. R. Stroberg, *Phys. Rev. Lett.* **117** (2016) 052501.
76. A. Ekstrom, G. R. Jansen, K. A. Wendt, G. Hagen, T. Papenbrock, B. D. Carlsson, C. Forssn, M. Hjorth-Jensen, P. Navrtil and W. Nazarewicz, *Phys. Rev. C* **91** (2015) 051301.
77. B. D. Carlsson, A. Ekstrom, C. Forssn, D. F. Strmberg, G. R. Jansen, O. Lilja, M. Lindby, B. A. Mattsson and K. A. Wendt, *Phys. Rev. X* **6** (2016) 011019.
78. B. A. Brown, S. Typel and W. A. Richter, *Phys. Rev. C* **65** (2002) 014612.
79. R. F. Garcia Ruiz *et al.*, *Nat. Phys.* **12** (2016) 594.
80. S. R. Stroberg, H. Hergert, J. D. Holt, S. K. Bogner and A. Schwenk, *Phys. Rev. C* **93** (2016) 051301(R).
81. S. R. Stroberg, A. Calci, H. Hergert, J. D. Holt, S. K. Bogner, R. Roth and A. Schwenk, *Phys. Rev. Lett.* **118** (2017) 032502.
82. W. A. Richter and B. A. Brown, *Phys. Rev. C* **80** (2009) 034301.
83. P. J. Ellis and T. Engeland, *Nucl. Phys. A* **144** (1970) 161; **A181** (1972) 368.
84. T. Engeland, *Nucl. Phys.* **72** (1965) 68.
85. G. E. Brown and A. M. Green, *Nucl. Phys.* **75** (1966) 401; **85** (1966) 87.
86. G. E. Brown and A. M. Green, *Phys. Lett.* **15** (1965) 168.
87. T. Erikson, K. F. Quader, G. E. Brown and H. T. Fortune, *Nucl. Phys. A* **465** (1987) 123.
88. T. Erikson, *Nucl. Phys. A* **170** (1971) 513; *Nucl. Phys. A* **211** (1973) 105.
89. A. Arima, H. Horiuchi and T. Sebe, *Phys. Lett. B* **24** (1967) 129.
90. J. P. Elliott, *Proc. R. Soc. A* **245** (1958) 129; J. P. Elliott and M. Harvey, *Proc. R. Soc. A* **272** (1963) 557.
91. R. Bansal and J. B. French, *Phys. Lett.* **11** (1964) 145; L. Zamick, *Phys. Lett.* **19** (1965) 580.
92. H. T. Fortune, *Phys. Rev. C* **18** (1978) 1053.
93. A. P. Zuker, B. Buck and J. B. McGrory, *Phys. Rev. Lett.* **21** (1968) 39.
94. A. P. Zuker, *Phys. Rev. Lett.* **23** (1969) 983.
95. E. K. Warburton, B. A. Brown and D. J. Millener, *Phys. Lett. B* **293** (1992) 7.
96. Y. Utsuno and S. Chiba, *Phys. Rev. C* **83** (2011) 021301(R).
97. R. Bijker and F. Iachello, *Nucl. Phys. A* **957** (2017) 154.